The Journal of Chemical Physics

Experimental and theoretical study of energy transfer in a chromophore triad: What makes modeling dynamics successful?

Cite as: J. Chem. Phys. **153**, 244114 (2020); https://doi.org/10.1063/5.0028126
Submitted: 02 September 2020 . Accepted: 04 December 2020 . Published Online: 28 December 2020

Victor M. Freixas, Tammie Nelson, Dianelys Ondarse-Alvarez, Parmeet Nijjar, Alexander Mikhailovsky, Cheng Zhou, Sebastian Fernandez-Alberti, Guillermo C. Bazan, and Sergei Tretiak

The Journal of Chemical Physics ARTICLE scitation.org/journal/jcp

Experimental and theoretical study of energy transfer in a chromophore triad: What makes modeling dynamics successful?

Cite as: J. Chem. Phys. 153, 244114 (2020); doi: 10.1063/5.0028126
Submitted: 2 September 2020 • Accepted: 4 December 2020 •
Published Online: 28 December 2020

Victor M. Freixas,[1] Tammie Nelson,[2,a)] Dianelys Ondarse-Alvarez,[1] Parmeet Nijjar,[3] Alexander Mikhailovsky,[4] Cheng Zhou,[5] Sebastian Fernandez-Alberti,[1,b)] Guillermo C. Bazan,[4] and Sergei Tretiak[2,6,c)]

AFFILIATIONS

[1]Universidad Nacional de Quilmes/CONICET, Roque Saenz Peña 352, B1876BXD Bernal, Argentina
[2]Physics and Chemistry of Materials, Theoretical Division, Los Alamos National Laboratory, Los Alamos, New Mexico 87545, USA
[3]Department of Chemistry, University of Southern California, Los Angeles, California 90089-1062, USA
[4]Department of Chemistry and Biochemistry, Center for Polymers and Organic Solids, University of California Santa Barbara, Santa Barbara, California 93106, USA
[5]Department of Chemistry, National University of Singapore, Singapore 117543, Singapore
[6]Center for Integrated Nanotechnologies, Los Alamos National Laboratory, Los Alamos, New Mexico 87545, USA

Note: This paper is part of the JCP Special Topic on Excitons: Energetics and Spatio-Temporal Dynamics.
[a)]**Author to whom correspondence should be addressed:** tammien@lanl.gov
[b)]**Electronic mail:** sfalberti@gmail.com
[c)]**Electronic mail:** serg@lanl.gov

ABSTRACT

Simulation of electronic dynamics in realistically large molecular systems is a demanding task that has not yet achieved the same level of quantitative prediction already realized for its static counterpart. This is particularly true for processes occurring beyond the Born–Oppenheimer regime. Non-adiabatic molecular dynamics (NAMD) simulations suffer from two convoluted sources of error: numerical algorithms for dynamics and electronic structure calculations. While the former has gained increasing attention, particularly addressing the validity of *ad hoc* methodologies, the effect of the latter remains relatively unexplored. Indeed, the required accuracy for electronic structure calculations to reach quantitative agreement with experiment in dynamics may be even more strict than that required for static simulations. Here, we address this issue by modeling the electronic energy transfer in a donor–acceptor–donor (D–A–D) molecular light harvesting system using fewest switches surface hopping NAMD simulations. In the studied system, time-resolved experimental measurements deliver complete information on spectra and energy transfer rates. Subsequent modeling shows that the calculated electronic transition energies are "sufficiently good" to reproduce experimental spectra but produce over an order of magnitude error in simulated dynamical rates. We further perform simulations using artificially shifted energy gaps to investigate the complex relationship between transition energies and modeled dynamics to understand factors affecting non-radiative relaxation and energy transfer rates.

I. INTRODUCTION

As interest in photoactive materials continues,[1–6] the demand for theoretical modeling to complement experiments[7] has led to a rapid growth in the field of excited state non-adiabatic molecular dynamics (NAMD) simulations, addressing the evolution of photoexcitations in realistic materials. Non-adiabatic dynamics underlies many relevant photophysical and photochemical processes such

as charge and/or energy transfer (ET), isomerization, exciton decay, and recombination, to name a few. These electronic non-adiabatic processes frequently occur in regions of phase space where excited state potential energy surfaces (PESs) become very close in energy or cross.[8] Thus, NAMD simulations must describe sophisticated processes beyond the Born–Oppenheimer approximation, giving rise to several challenges. One part of the problem is the increased complexity of dynamics algorithms when coupling electronic and nuclear degrees of freedom.[9] Another challenge is the need for an ensemble of trajectories each propagated for ten thousand (or more) time steps and requiring accurate quantum-chemical calculations of multiple excited states (i.e., energies, gradients, and non-adiabatic couplings) at each time step ($\sim 10^7$ single point calculations). This leads to a huge numerical expense for NAMD simulations compared to classical dynamics.[10] Clearly, the NAMD modeling of large molecular systems demands compromises to balance accuracy and numerical cost.[7,11] Thus, there are two main sources of error in NAMD simulations, specifically, approximations introduced in dynamics algorithms and electronic structure. These compounding errors must both be considered in order to successfully model dynamics.

First, numerous NAMD dynamics algorithms have been developed over the years from fully quantum[12,13] to mixed quantum-classical (MQC)[14] approaches. The MQC methods are well-suited for simulating realistically large molecular materials. Within this category, surface hopping methods largely dominate the field of NAMD simulations of photoactive materials.[15–21] In particular, the fewest switches surface hopping (FSSH)[22] algorithm is relatively simple, computationally inexpensive, and versatile. The FSSH algorithm was first introduced by Tully in 1990[22] as an approximate method for correlated electron-nuclear dynamics beyond the Born–Oppenheimer approximation. However, given that it cannot be formally derived from first-principles, the FSSH algorithm is considered *ad hoc*, and the reliability of FSSH results has been the subject of extensive studies leading to the development of a variety of alternative approaches. Nevertheless, there is broad evidence that validates this algorithm as an efficient NAMD method, achieving reasonable agreement with experimental measurements for a variety of molecular systems. While we cannot go into details about different NAMD methods and their approximations, we refer the reader to relevant recent reviews.[17,19,23] Furthermore, FSSH requires sampling of both molecular conformations and the non-deterministic wavepacket evolution. This is typically achieved simultaneously by propagating an ensemble of trajectories, making the results sensitive to statistical sampling and the number of trajectories in the ensemble. Past studies[11] have shed some light on the effects of statistical sampling and convergence in FSSH simulation results. A variety of previous studies aimed to improve FSSH accuracy by introducing, for example, decoherence[23–33] or trivial crossing[34–39] corrections. Thus, sources of error in NAMD dynamics algorithms are well quantified.[19] For example, the Ehrenfest and multiple cloning methods lead to around 10%–15% deviation from surface hopping.[19,40,41] Other sources of error in surface hopping (such as sampling and statistical or stochastic errors) are also well quantified,[11,19] being on the order of 10%.

On the other hand, for electronic structure calculations, multiple methods can be applied ranging from high-accuracy *ab initio* approaches[42–44] to semiempirical techniques.[45,46] Here, the time-dependent self-consistent field (TD-SCF) framework, such as time-dependent density functional theory (TD-DFT)[47,48] or time-dependent Hartree–Fock (TD-HF),[49,50] is popular, owing to the ability to treat realistic molecular sizes. Reduced numerical expense leads to inaccurate simulations where errors on the order of ±0.20 eV for absolute transition energies computed using TD-SCF approaches are typically considered as quantitatively accurate for modeling UV-spectra.[51–53] Here and throughout, we use "transition energy" to refer to the energy of transition between two electronic states. However, it is not entirely obvious whether the requirements for the electronic structure method underlying the NAMD simulations should be the same as those for static simulations. Since the non-adiabatic coupling scales inversely with the energy separation between states ($\sim 1/\Delta E$),[54,55] an energy shift of 0.1 eV, which is perfectly acceptable in modeling spectra, may cause non-radiative relaxation rates simulated using NAMD to vary by orders of magnitude. The manifestation of such errors in NAMD simulations is not at all straightforward, and as of yet, very little progress has been made toward understanding how inaccuracies in electronic structure calculations are propagated in dynamics. This problem is already recognized in the particular case of charge-transfer (CT) states. There, the appearance and relative energy alignment of spurious dark CT states depends strongly on the choice of the electronic structure method and has a significant effect on excited state dynamics.[56,57] To address this question, we focus our attention on a recently synthesized small light harvesting molecular donor, *p*-DTS(BT_2Th_3)$_2$ (referred to as MC2). The molecular structure, shown in Fig. 1(a), is comprised of dithienosilole (DTS),[58] 5-fluoro-2,1,3-benzothiadiazole (BT),[59] and thiophene (Th)[58] moieties. The donor–acceptor–donor (D–A–D) triad structure of MC2 consists of so-called "wing" (donor) and "core" (acceptor) units, identified in Fig. 1(a). The MC2 system is representative of many other conjugated organic systems in which the energy transfer occurs between donor and acceptor moieties.[60–62] Notably, such D–A systems exhibit characteristic absorbance spectra comprised of linear superpositions of the absorption of component pieces, often with strong overlap,[63,64] as will be demonstrated below for MC2. The MC2 system also has the benefit of having all bright states appearing in the absorption spectrum, and well-known complications arising from charge-transfer states[56,57] are avoided.

Here, we use time-resolved spectroscopic probes and excited state NAMD simulations based on the FSSH algorithm to investigate the non-radiative relaxation dynamics and concurrent electronic energy transfer in the MC2 complex. Photoluminescence (PL) and transient absorption (TA) spectroscopies detailed here suggest an efficient wing-to-core energy transfer on picosecond timescales following photoexcitation of the MC2 complex. Our study reveals how the accuracy of the electronic structure, reflected in the computed energy gap between states, influences the simulated dynamics and predicted energy transfer timescales compared to our reference experimental data. In Sec. II, we present experimental and computational methods used for spectroscopic measurements and NAMD modeling, respectively. In Sec. III, we present the results of our detailed spectroscopic investigations, which reveal the characteristic timescales and mechanisms underlying the energy transfer in MC2. We also present the results of our theoretical NAMD modeling of energy transfer and evaluate their accuracy compared to our reference experimental data. Section IV presents our conclusions

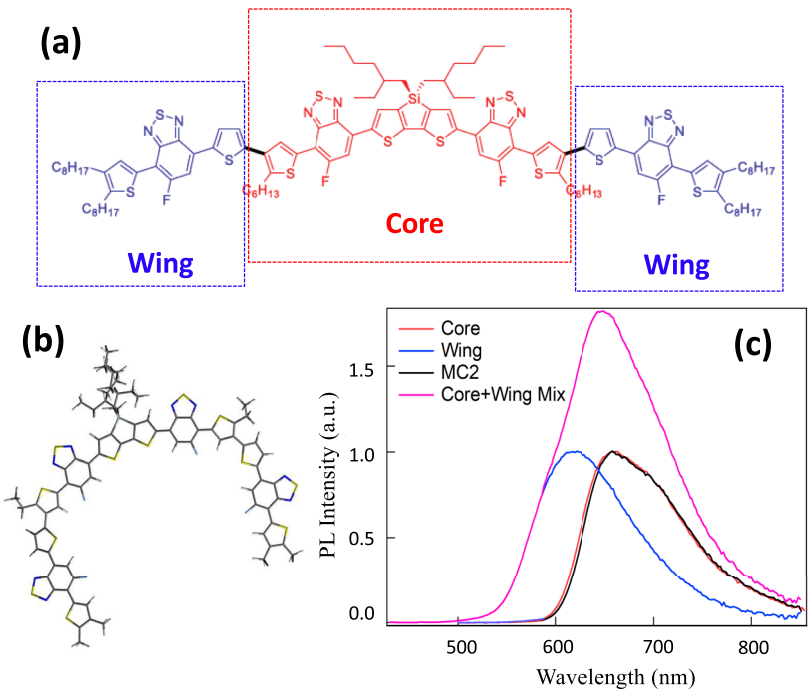

FIG. 1. (a) Chemical structure of the MC2 D–A–D molecular triad system comprised of wing and core units. (b) AM1 optimized ground state minimum energy structure revealing a horseshoe configuration. (c) Experimental photoluminescence (PL) spectra of the MC2 complex (black), isolated core (red), and isolated wing (blue) in the toluene solution following excitation at 320 nm. The convolution of wing and core emission spectra is also plotted (magenta).

and precautions for achieving accurate NAMD modeling for the class of D–A conjugated organic systems.

II. EXPERIMENTAL AND COMPUTATIONAL METHODS

A. UV-Vis and photoluminescence spectroscopy

All the molecules in this study were synthesized in house. All experiments were carried out in dilute ($<10^{-6}$M) degassed solutions of toluene, and measurements were conducted at room temperature (294 K). Kinetics analysis was performed using standard techniques and fitting functions (see the supplementary material). UV–Vis absorption spectra were collected on the Shimadzu UV-2401 spectrophotometer, and titration experiments were performed to determine molar absorptivity of the materials.[65] Photoluminescence (PL) and PL excitation spectra were recorded using the PTI Quantamaster fluorimeter. The PL quantum yield (PLQY) was determined relative to cresyl violet in methanol (PLQY = 54%)[66] and Rhodamine B in ethanol (PLQY = 49%)[67] using standard methodology.[68] Time-resolved PL lifetime measurements were performed using excitation at 400 nm, where all three species exhibit optical absorption [Fig. 4(a)]. A home-made time-correlated single photon counting (TCSPC)[69] spectrometer was used (see Ref. 70 for a detailed description). TCSPC PL decay traces were deconvoluted from the instrumental response function (IRF). Using the deconvolution procedure, it is possible to resolve processes taking place on the sub-IRF width timescale. Here, our estimated instrument response function FWHM (Full Width at Half Maximum) is 30 ps. However, the accuracy of the deconvoluted data depends on the *a priori* defined biexponential decay model.

B. Transient absorption spectroscopy

Transient absorption (TA) pump–probe experiments utilized a setup based on the system developed by Klimov and McBranch[71] with some modifications. The output of the regenerative amplifier is split into pump and probe arms with the pump beam being directed into an optical (Coherent Astrella) parametric amplifier (OPA, Topas Prime, Light Conversion) and a frequency mixer (NIRUVIS, Light Conversion) to produce required wavelengths. The OPA/frequency mixer output beam is then directed through a computer-controlled optical delay line and focused onto the sample. The probe beam is attenuated to the μJ level and is focused on a sapphire plate to produce fs supercontinuum capable of probing photoinduced absorption changes in the range of 440–1400 nm. The supercontinuum is overlapped with the pump spot on the sample by a parabolic mirror at a small angle and routed through a monochromator onto a photodiode detector (Si pin-photodiode for the range of 440–950 nm and InGaAs photodiode for the range of 950–1400 nm). The pump beam is modulated by an optical chopper at the first subharmonic frequency of the laser repetition rate. The photodiode signal is fed through a transimpedance amplifier into a lock-in amplifier synchronized with the chopper frequency to measure pump-induced optical transmission variation of the sample and into another lock-in amplifier synchronized with the full laser repetition rate to measure unperturbed optical transmission of the sample. The pump–probe delay and the monochromator wavelength are controlled by a computer to collect single-wavelength TA kinetics and time-resolved spectra. The setup is capable of measuring differential transmission signals (defined as the ratio of the photoinduced transmission coefficient change to the steady state transmission coefficient, $\Delta T/T$) down to 10^{-5} with

sub-100 fs resolution and can perform real-time chirp correction of the data.[71]

TA experiments were conducted using pump pulses with a wavelength of 570 nm to excite exclusively core segments of MC2 molecules. An optical pump at 460 nm was used to target wing segments of MC2; however, it produced some core excitations as well [see UV–Vis absorption spectra in Fig. 4(a)]. The pump and probe beam relative polarizations were set at a "magic" angle of 54° to avoid artifacts related to the polarization anisotropy. The pump beam energy density was set at ~2–5 μJ/cm^2 to avoid excitation density-dependent effects. The absence of the power-dependent phenomena was verified by collecting TA traces at several levels of the excitation density. Multiphoton phenomena were not observed. The laser repetition rate was set to 5 kHz, and no photoinduced degradation of the samples was detected.

C. Non-adiabatic molecular dynamics

Photoexcited dynamics is modeled using non-adiabatic molecular dynamics (NAMD). For this purpose, we employ the Non-Adiabatic Excited State Molecular Dynamics (NEXMD) software.[10,11,24,35,72,73] NEXMD uses the FSSH algorithm to efficiently model the non-radiative relaxation through multiple coupled electronic excited states in large molecular systems. An ensemble of independent trajectories is propagated, and within each trajectory, the nuclei are treated classically with forces from a single adiabatic excited state PES. Transitions (hops) among coupled excited states depend on the strength of the non-adiabatic couplings. Meanwhile, electrons are described quantum mechanically, requiring the calculation of excited state energies, analytical gradients, and non-adiabatic couplings.[10,74–78] The Collective Electronic Oscillator (CEO) approach[79,80] is used to compute excited states at the configuration interaction singles (CIS)[81] level of theory coupled with the semiempirical AM1 Hamiltonian[46] to decrease the numerical demand associated with treating large molecular systems. During NAMD simulations, the spatial energy transfer (electronic energy redistribution) can be followed via the time-dependent localization of the electronic transition density (TD). The orbital representation of the diagonal elements, $(\rho_{0\alpha})_{nn} = \langle\phi_0|c_n^\dagger c_n|\phi_\alpha\rangle$,[82,83] in atomic orbital (AO) basis functions n, provides a convenient analysis of the excited state wavefunction distribution in space. Here, ϕ_0 and ϕ_α are the ground and excited state adiabatic wavefunctions, respectively, and $c_n^\dagger c_n$ are the creation/annihilation operators on the AOs. By partitioning the MC2 molecule into donor/acceptor units corresponding to wing and core segments, the fraction of transition density, $(\rho^{0\alpha}(t))_X^2$, localized on each unit (X) at any given time is calculated by summing the contributions of the AOs from each atom (A) in a unit according to $(\rho^{0\alpha}(t))_X^2 = \sum_{n_A m_A}(\rho_{n_A m_A}^{0\alpha}(t))^2$.

D. Simulation details

NAMD simulations are performed for a single MC2 molecule in the gas phase. To reduce computational cost, we replace all of the $-C_8H_{17}$ sidechains in MC2 [see Fig. 1(a)] with $-CH_3$ groups on the wings and $-C_2H_5$ groups on the core. We start by running a 1 ns ground-state (GS) MD trajectory of MC2 starting from the GS minimum energy structure [shown in Fig. 1(b)]. GS dynamics was also performed for the isolated gas phase wing and core chromophores to simulate absorption spectra. GS dynamics was performed using constant temperature Langevin propagation[84,85] at 300 K with a time step of 0.5 fs and a friction coefficient of 20 ps^{-1}. From the equilibrated GS trajectories, 325 snapshots of nuclear geometries and velocities were sampled to provide initial conditions for excited state dynamics (MC2) and/or configurations for simulated absorption spectra (MC2, wing, and core). For each sampled configuration, excited state energies and oscillator strengths were computed for six lowest energy excited states to produce an average absorption spectrum. The contribution to the total spectrum from each excited state is modeled using a Gaussian line shape with a spectral broadening of 0.05 eV.

The initial excited state for NAMD simulations was selected stochastically according to a Gaussian shaped Frank–Condon window centered at 465 nm. A Gaussian laser pulse is used, $f(t) = \exp(-t^2/2T^2)$, with T = 42.5 fs corresponding to a FWHM of 100 fs. Excited state trajectories were then propagated for 2 ps at constant energy with a classical time step of 0.1 fs and a quantum time step of 0.025 fs where five lowest energy excited states were included in the simulations. While the conformational sampling is performed using a classical Langevin thermostat after reaching equilibrated 300 K conditions, constant energy simulations are more appropriate for the description of ultrafast, non-equilibrium processes involving an initially large excess of energy introduced by photoexcitation. The instantaneous decoherence correction[24] was used to account for divergent wavepackets. Trivial unavoided crossings were detected by reducing the quantum time step by a factor of 40 to eliminate any unphysical energy transfer associated with nuclear rearrangements that cause the adiabatic ordering of states to change in time.[35,85] The NAMD simulations were performed using native (AM1/CIS) energies as well as adjusted S_i–S_1 energy gaps achieved by increasing the energy of all states above S_1 by uniform shift energy E_{shift} = 0.25 eV, 0.50 eV, 1.00 eV according to $E_i^{shift} = E_i + E_{shift}$ for all $i > 1$.

III. RESULTS

A. Photoluminescence and transient absorption spectroscopies

Steady state photoluminescence (PL) spectra of the MC2 complex and isolated wing and core chromophores (i.e., isolated wing and core molecules not joined together) have been measured following excitation at 320 nm, as shown in Fig. 1(c). A mixed emission profile from both wing and core units would yield a spectrum similar to the convolution (magenta). Instead, the emission from the MC2 complex (black) coincides with the emission of the isolated core moiety (red) and no emission is observed in the wavelength range associated with PL emission from the wing component (blue). PLQE (quantum efficiency) values determined for the isolated core, wing, and MC2 samples are 33%, 100%, and 36%, respectively. The complete absence of PL emission from the wing component and PL excitation spectra matching that of UV–Vis absorption in MC2 (Fig. S1) points to a nearly 100% efficient energy transfer (ET) between the wing and core components of MC2. During this process, part of the initial photoexcitation energy is lost to vibrational excitation due to non-radiative relaxation. To investigate this

hypothesis, time-resolved PL measurements were conducted to visualize kinetics of the excited states in MC2 and its isolated components. The results for MC2, shown in Fig. 2(a), reveal monoexponential decay of PL with a time constant of 1.65 ns in the mid to long-wavelength side of the emission spectrum. However, on the short-wavelength side of the PL spectrum, MC2 exhibits a fast initial component of PL decay [Fig. 2(b)], consistent with the hypothesis of intramolecular ET. Analysis of the fast PL decay on the high energy side of the spectrum and its complementary onset on the low energy side revealed exponential ET kinetics with a time constant of 36 ps. While the PL experiments unambiguously indicate the presence of the ET process and enable one to estimate the order of magnitude for its time constant to provide more reliable data, we used TA spectroscopy with temporal resolution <100 fs, described below.

Detailed kinetics of excited states was studied via TA pump–probe spectroscopy. The origin of the TA signals has been discussed in detail elsewhere. For example, TA signals are analyzed by multiple methods ranging from simple rate equations for single wavelength kinetics to complicated global fitting approaches.[86] Here, we utilize the former approach for simplicity. The model used for the analysis of the data is provided in the supplementary material. TA spectra show ground state bleaching (GSB) and stimulated emission (SE) bands coinciding with steady state absorption band and PL spectra, respectively. Photoinduced excited state absorption has not been detected in the probed range of the spectrum due to either cancellation by intense GSB and SE signals or low energy of this transition lying outside of the range probed. The decay of these bands is monoexponential with time constants similar to those determined in the transient PL experiments. Excitation of MC2 at 470 nm (mixed wing/core absorption) is consistent with ET, as seen in Fig. 2(c), where TA spectra at 0.78 ps and 20 ps show the spectral shift and delayed growth of the SE band associated with the core excited state of MC2. Linear scale plots of the TA transients are provided (Fig. S2) to aid in interpretation of data around time t = 0 (i.e., close to the pulse width). A comparison of the core SE band kinetics in MC2 under 460 nm (wing) and 570 nm (core) excitation is shown in Fig. 2(d). At 570 nm, all excited states are generated directly on the core unit and the SE band at 700 nm (core) exhibits a fast, excitation pulse duration-limited rise. With 460 nm excitation, a significant fraction of excited states is initially localized on the wing segment, resulting in a slower onset of the SE signal at 700 nm associated with the core. Therefore, an efficient energy transfer to the core unit occurs following photoexcitation of the MC2 complex at 460 nm, in accordance with Kasha's rule.[87] A simple bi-exponential fit [inset of Fig. 2(d)] of the onset of the MC2 SE band yields ET time constants of 2.7 ps and 37 ps with relative weights of 0.7 and 0.3, respectively. The fit also indicates that about 50% of excited states are generated on the wing segments.

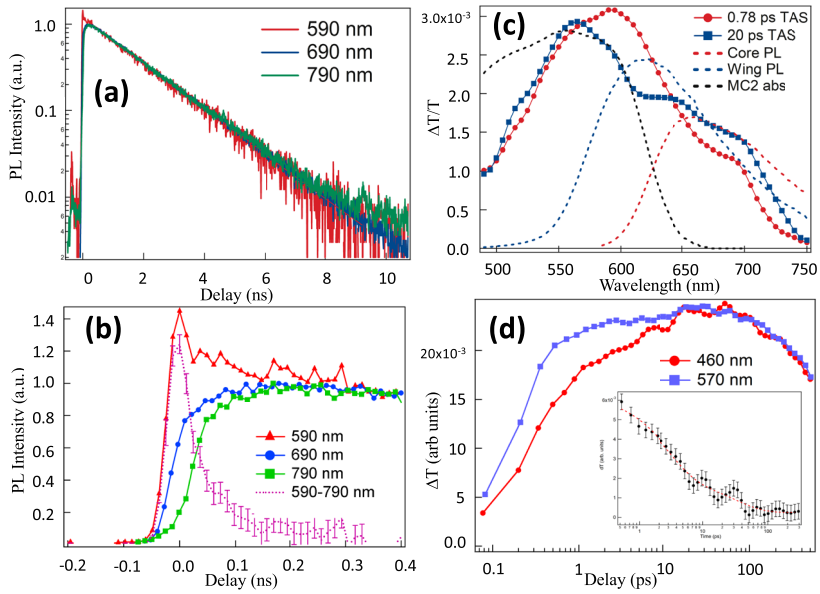

FIG. 2. (a) PL transients (logarithmic scale) collected at different wavelengths in the MC2 toluene solution, excited at 400 nm. (b) Early time PL transients in the MC2 toluene solution excited at 400 nm, collected at different wavelengths. The difference between 590 nm and 790 nm kinetics (magenta dashes) provides a rough visualization of the ET process. (c) TA spectra of MC2 in toluene excited at 470 nm plotted as differential transmission signals, ΔT/T (unitless). Core (red dashes) and wing (blue dashes) PL spectra and MC2 absorption (black dashes) are provided as reference. The TA spectrum at 0.78 ps delay (red circles) has several bleaching bands. The peak near 600 nm matches the position of the wing PL peak and corresponds to the SE band generated by excitations localized on the wing segment of MC2. The TA spectrum at 20 ps delay (blue squares) shows the SE band at 600 nm (wing) vanishes and the peak around 700 nm (core) grows. The 700 nm peak is attributed to the SE band produced by the excited core in MC2, demonstrated by the overlap with core PL. (d) TA transients in the MC2 toluene solution collected at 700 nm (Core SE band) under direct core excitation (570 nm) and mixed core/wing excitation (460 nm). Here, single wavelength transients are plotted as normalized transmission change ΔT vs delay time (logarithmic scale). The inset shows the extracted ET trace and biexponential fit with error bars.

B. Excited state localization and optical spectra

We analyze the spatial localization of the five lowest energy excited states in the MC2 complex. The state transition densities at the optimized GS configuration, plotted in Fig. 3, confirm that wing and core units of the MC2 macromolecule behave as separate chromophores that spatially localize electronic excitations. $S_{1/4/5}$ are localized within the core unit, whereas $S_{2/3}$ are quasi-degenerate states localized within the wings (the subscripts used here and throughout refer to adiabatic state ordering). The inherent energy gradient suggests a concerted energy redistribution and change in spatial localization between wing and core units following photoexcitation.

Before performing NAMD simulations, it is essential to verify that the electronic structure method provides an accurate description of the excited state energies. In particular, when modeling NAMD in large, realistic conjugated organics, the choice of electronic structure methods quickly becomes limited. For the class of light harvesting conjugated organics similar to MC2, semiempirical techniques have been demonstrated to perform at the same level as TD-DFT, producing a similar error of ~0.20 eV. Thus, it is a common routine to rely on the comparison of calculated absorption spectra and experimental UV–Vis data to benchmark electronic structure methods.

The absorption spectra of MC2 and the isolated core and wing moieties have been experimentally measured, as shown in Fig. 4(a). As expected, the MC2 absorption spectrum can be described as a linear superposition of the absorption spectra of its components. The experimentally derived ratio of the molecular moieties differs from the ideal 1:2 value (Fig. S3) probably due to the change of transition dipoles after assembly of core and wing components into the MC2 molecule. The AM1/CIS calculated absorption spectrum is plotted in Fig. 4(b) where the individual states have been summed according to their localization in either wing ($S_{2/3}$) or core ($S_{1/4/5}$) to reveal the contribution from each unit. The calculated absorption shows good quantitative agreement with the experimental spectra. Here, all of the main absorption features in the experimental spectrum and their absolute energies are reproduced in the calculated spectrum. The feature resembling a vibronic structure in the experimental MC2 spectrum is due to the presence of two distinct optically active electronic states with distinct vibrational manifolds. From the experimental spectrum, the peak wing absorption occurs at 460 nm (2.69 eV) and the peak core absorption arises at 570 nm (2.17 eV). In comparison, the peak wing absorption is predicted to be 470 nm (2.64 eV) and the peak core absorption is predicted to be 560 nm (2.21 eV), being well within the accepted energy tolerance for static excited state electronic structure calculations varying by no more than 0.05 eV from the experimental values.

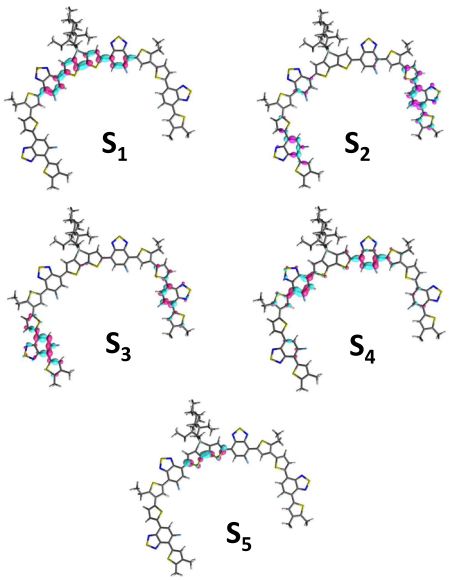

FIG. 3. Orbital plots of the transition density for the five lowest energy electronic states at the optimized GS geometry reveal localization of S_1, S_4, and S_5 on the core and S_2 and S_3 on the wings.

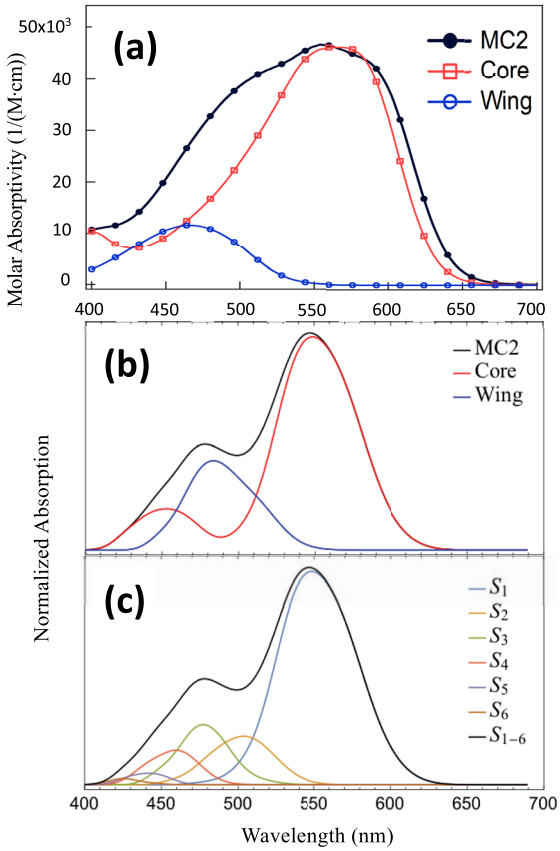

FIG. 4. (a) Experimental UV–Vis absorption spectra of MC2 (black) and isolated core (red) and wing (blue) molecules in toluene expressed in molar absorptivity units. (b) Calculated absorption spectrum of MC2 (black) at 300 K using six excited states, showing contributions from wing (blue) and core (red) localized states. (c) Calculated absorption spectrum of MC2 at 300 K using six excited states, showing contributions from individual states S_1–S_6.

C. Electronic dynamics and energy transfer

Based on the "good" agreement in the static electronic structure shown above, we next proceed to NAMD simulations. The calculated absorption of wing and core components in Fig. 4(b) is strongly overlapping. Because of this, the state initially populated in NAMD simulations by excitation at 465 nm varies from S_1 to S_5 (see Table S1 in the supplementary material), resulting in a mixture of wing and core localized states, which is also the case for experimental time-resolved spectroscopy (see above). However, the initial excitation is primarily dominated by the quasi-degenerate wing-localized S_3 and S_2 states comprising 88.9% of configurations. The non-radiative relaxation process results in the decay of adiabatic state populations from the initially populated state to the lowest energy S_1 state, plotted in Fig. 5(a), confirming the scenario of energy transfer to the core. According to FSSH prescription, the populations are computed as the fraction of trajectories evolving on a given state. In general, the population of states $S_{2/3/4/5}$ immediately decays, while the population is accumulated in S_1. Next, we consider the energy transfer between wing and core units by analyzing the average fraction of transition density (TD) localized in wing and core units during the relaxation dynamics. The ensemble average (including all 325 trajectories) of the time evolution of the fraction of TD is shown in Fig. 5(b). Here, it is important to note that there is considerable conformational variation observed during ground state dynamics at room temperature used for sampling of initial conditions, as evidenced by the distribution of sampled dihedral angles between wing and core units spanning a range of 0°–90°. In addition, the dihedral angles between wing and core units rotate freely during the non-radiative relaxation dynamics (Fig. S4). Due to the initial conformational variation and the distribution of initially populated states (discussed above), the initial TD is ~60% localized on the wing units and ~40% localized in the core unit.

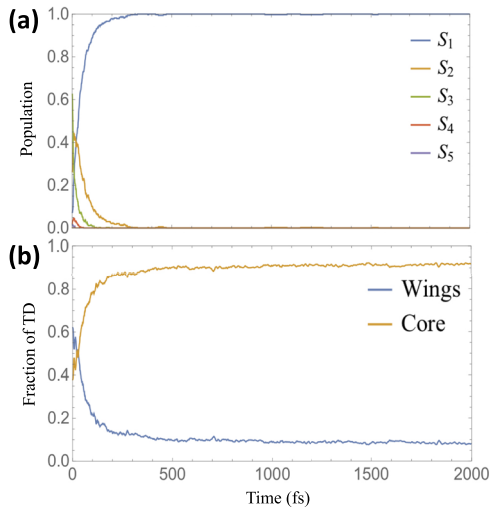

FIG. 5. (a) Time evolution of adiabatic state populations during NAMD simulation of MC2 using the native S_i–S_1 energy gap. (b) Corresponding time evolution of the fraction of TD localized in wing and core units averaged over the ensemble of 325 trajectories.

This is in agreement with an approximately equal initial population of core and wing states seen in spectroscopic TA experiments (see the supplementary material) upon excitation of MC2 at 460 nm. The TD undergoes transfer rapidly leaving the wing and becoming more than 90% localized in the core unit after 2 ps. The associated timescale for the energy transfer qualitatively follows the relaxation of adiabatic state populations, confirming that the energy transfer coincides with the non-adiabatic transition to S_1. The overall energy transfer timescale, τ, is found by fitting the fraction of TD localized within the wing to an exponential decay function $f(t) = a - be^{-\left(\frac{t}{\tau}\right)}$. We find an energy transfer timescale of 79.2 ± 0.6 fs for the change in localization from the wings to the core.

D. Electronic structure effects in NAMD

Clearly, the predicted ultrafast sub-100 fs energy transfer timescale does not agree with either characteristic timescales (2.7 ps and 37 ps) observed via TA spectroscopy. The predicted timescale differs by over an order of magnitude. This error is much larger than ~10% expected from NAMD dynamics algorithms.[11,19] Therefore, we conclude that the main source of error must originate from the electronic structure. To understand this discrepancy, we must take a closer look at the calculated absorption spectrum, this time considering the contribution of individual excited states, as seen in Fig. 4(c). There is a continuous band of strongly overlapping bright states, which gives rise to the predicted spectral shape. The spatial energy transfer in MC2 should coincide with the moment of non-adiabatic transition between wing and core localized states[88] confirmed in Fig. 5. Thus, the relevant energy gaps are between the lowest energy wing-localized states (S_3 and S_2) and the lowest energy core-localized state (S_1). From the individual contributions in Fig. 4(c), the average theoretical energy gaps for S_3–S_1 and S_2–S_1 are 0.37 eV and 0.27 eV, respectively, with peaks being centered at 560 nm (S_1), 500 nm (S_2), and 480 nm (S_3). In addition, the absorption contributions of S_{1-3} are very broad and strongly overlapping so that the effective theoretical wing–core energy gaps can be even smaller. Meanwhile, the estimated experimental wing–core energy gap is significantly larger, being 0.52 eV [Fig. 4(a)].

Despite this discrepancy, the predicted absolute peak energies and energy gap between wing and core bands [Fig. 4(b)] reproduce the experimental spectrum, giving us a false confidence in the accuracy of the electronic structure calculations applied to dynamics. NAMD simulations using the underestimated native energy gaps ΔE produce unrealistically fast relaxation and energy transfer timescale due to the $\sim 1/\Delta E$ scaling of the non-adiabatic coupling. Thus, we motivate an artificial increase of the S_i–S_1 energy gap in order to understand how underlying state distributions obtained from the electronic structure affect the modeled non-radiative relaxation dynamics. Based on the underestimated theoretical $S_{2/3}$–S_1 energy gap compared to the experimental spacing between wing and core bands, we increase the S_i–S_1 energy gap by 0.25 eV, 0.50 eV, and 1.00 eV to eliminate the overlap between calculated absorption bands of $S_{2/3}$ and S_1. We further motivate these shifts by noting that it is difficult to assess the actual experimental gap based on the broad absorption bands in Fig. 4(a).

Next, we repeat our NAMD simulations using shifted energy gaps. The evolution of adiabatic state populations and TD localization is plotted in Fig. S5, and the fitted energy transfer timescales are

TABLE I. Calculated wing → core energy transfer timescales for different energy gap shifts.

Shift (eV)	Timescale, τ (fs)
0.00	79.2 ± 0.6
0.25	191.0 ± 0.9
0.50	719 ± 5
1.00	—

summarized in Table I. As expected, we observe a dramatic dependence of the energy transfer rates on the shift. By opening the gaps, the $S_{2/3}$ and S_1 bands are getting separated and have less overlap, introducing a bottleneck in the relaxation. S_2 acts as an intermediate state whose population initially rises as the population transferred from $S_{3/4/5}$ is accumulated and then decreases as the $S_2 \rightarrow S_1$ transition takes over. The turnover of the S_2 population is shifted to later and later times, and relaxation to S_1 is slowed along with the corresponding energy transfer between the wing and core as the gap increases. The energy transfer for the largest 1.00 eV shift was slowed to such an extent that the exponential behavior was not achieved within the 2 ps simulation time. The 0.50 eV shift produces an energy transfer timescale in best agreement with the timescale observed in TA experiments.

IV. CONCLUSION

In summary, quantitative NAMD simulations are still a holy grail, largely due to the difficulty of controlling errors arising from both the algorithms used for dynamics and electronic structure methods. Because of the complex nature of modeling dynamics beyond the Born–Oppenheimer approximation, NAMD algorithms generally involve many assumptions and are often *ad hoc*. On the other hand, depending on the size of the system under investigation, the photophysical processes of interest, and their associated timescales, the electronic structure methods employed can range from high accuracy CAS-PT2 methods[89,90] (tens of atoms) to TD-DFT approaches[20,91,92] to semiempirical techniques[88,93,94] (hundreds of atoms). The accuracy of simulated dynamics depends on both of these factors making errors difficult to control. When agreement with experiment is achieved, it is unclear whether this is due to the accuracy of the method or simply a fortuitous cancellation of errors. We have performed extensive experimental characterization of the electronic energy transfer in the MC2 D–A–D molecular system using time-resolved spectroscopies. With these high fidelity data at hand, we further conducted excited-state NAMD modeling of spectra and energy transfer timescales using the FSSH method with native energy gaps (computed directly from the electronic structure method) and three adjusted energy gaps (shifted by a constant value; 0.25 eV, 0.50 eV, and 1.00 eV). Our simulations reveal the sensitivity of simulated energy transfer rates to changes in the computed transition energies. Here, native transition energies provide accurate modeling of absorption spectra with absolute peak energies for wing and core contributions varying by not more than 0.05 eV. However, this produces an ultrafast energy transfer orders of magnitude faster than the experimentally observed picosecond timescales. In a scenario where the $S_{2/3}$–S_1 gap is increased by 0.25 eV, the predicted timescale immediately increases from 79 fs to 191 fs. This case demonstrates that even though an error of ±0.2 eV in transition energies is acceptable for modeling static spectra, it is not a tight enough criterion for dynamics. Increasing the gap by 0.50 eV results in an even slower rate having a timescale of 719 fs. The effect seen here is similar to the observed sensitivity of rates due to the presence of a dielectric environment such as solvents.[95–99]

While we used the FSSH framework, our findings apply to many NAMD methods, especially within the MQC family, though the specific sensitivity to the accuracy of electronic structure still needs to be investigated for other approaches. Since the MC2 system is representative of other conjugated organic D–A type systems in which the energy transfer occurs, the results presented here should apply more generally to any molecule within this broad class of materials. The shifting of energy gaps is not recommended as a correction method; it is used here to demonstrate that electronic structure calculations can produce results that appear accurate but contain erroneous underlying state distributions that can contribute to significant error in NAMD results. Absorbance spectra are inexpensive, fast, reliable, easily accessible, and widely available in the literature or through experiment. They are, in practice, routinely used as a benchmark comparison for evaluating electronic structure calculations. For static calculations, this is generally an acceptable practice. However, overall, the criteria for quantitative dynamics simulations must be more stringent than those used for static simulations. In the ideal world, we would compare to many other metrics; however, these are not always available. To the contrary, with more and more NAMD software packages now being released, ambitious experimentalists and theorists will be tempted to use such tools as a black box. NAMD simulations have many areas for caution and delicate balances that must be finessed. In general, the modeler needs to be aware of the drastic sensitivity of dynamical rates that can be caused by small deviations in electronic structure results.

SUPPLEMENTARY MATERIAL

See the supplementary material for the following information: detailed description of the analysis method for experimental kinetics and energy transfer from TA spectroscopy, table of the distribution of states comprising the initial excitation (Table S1), photoluminescence excitation and optical absorption spectra in wing, core, and MC2 molecules (Fig. S1), short-time TA transients in MC2 plotted on a linear scale (Fig. S2), experimental UV–Vis absorption spectra of core, wing, and MC2 molecules showing the sum of core and wing spectra in 1:1 and 1:2 ratios (Fig. S3), distribution of dihedral angles sampled from ground state dynamics and evolution of dihedral angles during NEXMD simulations (Fig. S4), and evolution of adiabatic state populations and transition density localized on the wing and core for energy gap shifts of 0.25 eV, 0.50 eV, and 1.0 eV (Fig. S5).

ACKNOWLEDGMENTS

The work at Los Alamos National Laboratory (LANL) was supported by the LANL Directed Research and Development (LDRD)

Funds and performed in part at the Center for Nonlinear Studies (CNLS) and the Center for Integrated Nanotechnologies (CINT), a U.S. Department of Energy, Office of Science user facility at LANL. S.F.-A. was supported by CONICET, UNQ, ANPCyT (Grant No. PICT-2018-02360). The ultrafast laser instrumentation used for TA and TCSPC measurements was funded by DURIP ARO (Grant No. 66886LSRIP). This research used resources provided by the LANL Institutional Computing (IC) Program. LANL is operated by Triad National Security, LLC, for the National Nuclear Security Administration of the U.S. Department of Energy (Contract No. 89233218NCA000001).

DATA AVAILABILITY

The data that support the findings of this study are available within the supplementary material and from the corresponding author upon reasonable request.

REFERENCES

[1] *Novel Photoactive Materials*, edited by M. V. Diamanti (MDPI, Basel, Switzerland, 2019).
[2] Q. Shao and B. Xing, "Photoactive molecules for applications in molecular imaging and cell biology," Chem. Soc. Rev. **39**, 2835–2846 (2010).
[3] E. A. Rodriguez, R. E. Campbell, J. Y. Lin, M. Z. Lin, A. Miyawaki, A. E. Palmer, X. Shu, J. Zhang, and R. Y. Tsien, "The growing and glowing toolbox of fluorescent and photoactive proteins," Trend Biochem. Sci. **42**, 111–129 (2017).
[4] A. H. Gelebart, D. Jan Mulder, M. Varga, A. Konya, G. Vantomme, E. W. Meijer, R. L. B. Selinger, and D. J. Broer, "Making waves in a photoactive polymer film," Nature **546**, 632–636 (2017).
[5] B. Fan, X. Du, F. Liu, W. Zhong, L. Ying, R. Xie, X. Tang, K. An, J. Xin, N. Li, W. Ma, C. J. Brabec, F. Huang, and Y. Cao, "Fine-tuning of the chemical structure of photoactive materials for highly efficient organic photovoltaics," Nat. Energy **3**, 1051–1058 (2018).
[6] H. Wang, Y. Rahaq, and V. Kumar, "A composite light-harvesting layer from photoactive polymer and halide perovskite for planar heterojunction solar cells," Sci. Rep. **6**, 29567 (2016).
[7] I. Tavernelli, "Nonadiabatic molecular dynamics simulations: Synergies between theory and experiments," Acc. Chem. Res. **48**, 792–800 (2015).
[8] A. W. Jasper, C. Zhu, S. Nangia, and D. G. Truhlar, "Introductory lecture: Nonadiabatic effects in chemical dynamics," Faraday Discuss. **127**, 1–22 (2004).
[9] M. Ben-Nun, J. Quenneville, and T. J. Martínez, "Ab initio multiple spawning: Photochemistry from first principles quantum molecular dynamics," J. Phys. Chem. A **104**, 5161 (2000).
[10] T. Nelson, S. Fernandez-Alberti, V. Chernyak, A. E. Roitberg, and S. Tretiak, "Nonadiabatic excited-state molecular dynamics modeling of photoinduced dynamics in conjugated molecules," J. Phys. Chem. B **115**, 5402–5414 (2011).
[11] T. Nelson, S. Fernandez-Alberti, V. Chernyak, A. E. Roitberg, and S. Tretiak, "Nonadiabatic excited-state molecular dynamics: Numerical tests of convergence and parameters," J. Chem. Phys. **136**, 054108 (2012).
[12] M. H. Beck, A. Jäckle, G. A. Worth, and H. D. Meyer, "The multiconfiguration timedependent Hartree (MCTDH) method: A highly efficient algorithm for propagating wavepackets," Phys. Rep. **324**, 1–105 (2000).
[13] M. Ben-Nun and T. J. Martínez, "Ab initio quantum molecular dynamics," Adv. Chem. Phys. **121**, 439–512 (2002).
[14] J. C. Tully, "Mixed quantum classical dynamics," Faraday Discuss. **110**, 407–419 (1998).
[15] A. W. Jasper, S. Nangia, C. Zhu, and D. G. Truhlar, "Non-Born-Oppenheimer molecular dynamics," Acc. Chem. Res. **39**, 101–110 (2006).
[16] M. Barbatti, "Nonadiabatic dynamics with trajectory surface hopping method," Wiley Interdiscip. Rev.: Comput. Mol. Sci. **1**, 620–633 (2011).
[17] R. Crespo-Otero and M. Barbatti, "Recent advances and perspectives on nonadiabatic mixed quantum-classical dynamics," Chem. Rev. **118**, 7026 (2018).
[18] J. C. Tully, "Perspective: Nonadiabatic dynamics theory," J. Chem. Phys. **137**, 22A301 (2012).
[19] T. R. Nelson, A. J. White, J. A. Bjorgaard, A. E. Sifain, Y. Zhang, B. Nebgen, S. Fernandez-Alberti, D. Mozyrsky, A. E. Roitberg, and S. Tretiak, "Non-adiabatic excited-state molecular dynamics: Theory and applications for modeling photophysics in extended molecular materials," Chem. Rev. **120**, 2215–2287 (2020).
[20] L. Wang, A. Akimov, and O. V. Prezhdo, "Recent progress in surface hopping: 2011-2015," J. Phys. Chem. Lett. **7**, 2100–2112 (2016).
[21] L. Wang, O. V. Prezhdo, and D. Beljonne, "Mixed quantum-classical dynamics for charge transport in organics," Phys. Chem. Chem. Phys. **17**, 12395–12406 (2015).
[22] J. C. Tully, "Molecular dynamics with electronic transitions," J. Chem. Phys. **93**, 1061–1071 (1990).
[23] J. E. Subotnik, A. Jain, B. Landry, A. Petit, W. Ouyang, and N. Bellonzi, "Understanding the surface hopping view of electronic transitions and decoherence," Annu. Rev. Phys. Chem. **67**, 387–417 (2016).
[24] T. Nelson, S. Fernandez-Alberti, A. E. Roitberg, and S. Tretiak, "Nonadiabatic excited-state molecular dynamics: Treatment of electronic decoherence," J. Chem. Phys. **138**, 224111 (2013).
[25] A. Jain, E. Alguire, and J. E. Subotnik, "An efficient, augmented surface hopping algorithm that includes decoherence for use in large-scale simulations," J. Chem. Theory Comput. **12**, 5256–5268 (2016).
[26] H. M. Jaeger, S. Fischer, and O. V. Prezhdo, "Decoherence-induced surface hopping," J. Chem. Phys. **137**, 22A545 (2012).
[27] A. White, S. Tretiak, and D. Mozyrsky, "Coupled wave-packets for non-adiabatic molecular dynamics: A generalization of Gaussian wave-packet dynamics to multiple potential energy surfaces," Chem. Sci. **7**, 4905–4911 (2016).
[28] C. C. Martens, "Surface hopping by consensus," J. Phys. Chem. Lett. **7**, 2610–2615 (2016).
[29] G. Granucci, M. Persico, and A. Zoccante, "Including quantum decoherence in surface hopping," J. Chem. Phys. **133**, 134111 (2010).
[30] J. E. Subotnik, "Fewest-switches surface hopping and decoherence in multiple dimensions," J. Phys. Chem. A **115**, 12083–12096 (2011).
[31] C. Zhu, S. Nangia, A. W. Jasper, and D. G. Truhlar, "Coherent switching with decay of mixing: An improved treatment of electronic coherence for non-Born-Oppenheimer trajectories," J. Chem. Phys. **121**, 7658–7670 (2004).
[32] M. J. Bedard-Hearn, R. E. Larsen, and B. J. Schwartz, "Mean-field dynamics with stochastic decoherence (MF-SD): A new algorithm for nonadiabatic mixed quantum/classical molecular-dynamics simulations with nuclear-induced decoherence," J. Chem. Phys. **123**, 234106 (2005).
[33] J.-Y. Fang and S. Hammes-Schiffer, "Improvement of the internal consistency in trajectory surface hopping," J. Phys. Chem. A **103**, 9399–9407 (1999).
[34] L. Wang and O. V. Prezhdo, "A simple solution to the trivial crossing problem in surface hopping," J. Phys. Chem. Lett. **5**, 713–719 (2014).
[35] S. Fernandez-Alberti, A. E. Roitberg, T. Nelson, and S. Tretiak, "Identification of unavoided crossings in nonadiabatic photoexcited dynamics involving multiple electronic states in polyatomic conjugated molecules," J. Chem. Phys. **137**, 014512 (2012).
[36] G. A. Meek and B. G. Levine, "Evaluation of the time-derivative coupling for accurate electronic state transition probabilities from numerical simulations," J. Phys. Chem. Lett. **5**, 2351–2356 (2014).
[37] L. Wang, D. Trivedi, and O. V. Prezhdo, "Global flux surface hopping approach for mixed quantum-classical dynamics," J. Chem. Theory Comput. **10**, 3598–3605 (2014).
[38] E. M. Y. Lee and A. P. Willard, "Solving the trivial crossing problem while preserving the nodal symmetry of the wave function," J. Chem. Theory Comput. **15**, 4332–4343 (2019).
[39] X. Bai, J. Qiu, and L. Wang, "An efficient solution to the decoherence enhanced trivial crossing problem in surface hopping," J. Chem. Phys. **148**, 104106 (2018).
[40] D. V. Makhov, W. J. Glover, T. J. Martinez, and D. V. Shalashilin, "*Ab initio* multiple cloning algorithm for quantum nonadiabatic molecular dynamics," J. Chem. Phys. **141**, 054110 (2014).

[41] V. M. Freixas, S. Fernandez-Alberti, D. V. Makhov, S. Tretiak, and D. Shalashilin, "An *ab initio* multiple cloning approach for the simulation of photoinduced dynamics in conjugated molecule," Phys. Chem. Chem. Phys. **20**, 17762–17772 (2018).
[42] F. Plasser, S. A. Mewes, A. Dreuw, and L. González, "Detailed wave function analysis for multireference methods: Implementation in the Molcas program package and applications to tetracene," J. Chem. Theory Comput. **13**, 5343–5353 (2017).
[43] L. González, D. Escudero, and L. Serrano-Andrés, "Progress and challenges in the calculation of electronic excited states," ChemPhysChem **13**, 28–51 (2012).
[44] K. K. Baeck and T. J. Martinez, "Ab initio molecular dynamics with equation-of-motion coupled-cluster theory: Electronic absorption spectrum of ethylene," Chem. Phys. Lett. **375**, 299–308 (2003).
[45] W. Thiel, "Semiempirical quantum-chemical methods," Wiley Interdiscip. Rev.: Comput. Mol. Sci. **4**, 145–157 (2013).
[46] M. J. S. Dewar, E. G. Zoebisch, E. F. Healy, and J. J. P. Stewart, "The development and use of quantum mechanical molecular models. 76. AM1: A new general purpose quantum mechanical molecular model," J. Am. Chem. Soc. **107**, 3902 (1985).
[47] C. Adamo and D. Jacquemin, "The calculations of excited-state properties with time-dependent density functional theory," Chem. Soc. Rev. **42**, 845–856 (2013).
[48] M. A. L. Marques and E. K. U. Gross, "Time-dependent density functional theory," Annu. Rev. Phys. Chem. **55**, 427–455 (2004).
[49] P. Jorgensen, "Molecular and atomic applications of time-dependent Hartree-Fock theory," Annu. Rev. Phys. Chem. **26**, 359 (1975).
[50] A. D. McLachlan and M. A. Ball, "Time-dependent Hartree-Fock theory for molecules," Rev. Mod. Phys. **36**, 844 (1964).
[51] D. Jacquemin, E. A. Perpète, I. Ciofini, C. Adamo, R. Valero, Y. Zhao, and D. G. Truhlar, "On the performances of the M06 family of density functionals for electronic excitation energies," J. Chem. Theory Comput. **6**, 2071–2085 (2010).
[52] M. Caricato, G. W. Trucks, M. J. Wiberg, and K. B. Wiberg, "Electronic transition energies: A study of the performance of a large range of single reference density functional and wave function methods on valence and Rydberg states compared to experiment," J. Chem. Theory Comput. **6**, 370–383 (2010).
[53] A. E. Sifain, J. A. Bjorgaard, T. W. Myers, J. M. Veauthier, D. E. Chavez, O. V. Prezhdo, R. J. Scharff, and S. Tretiak, "Photoactive excited states in explosive Fe(II) tetrazine complexes: A time-dependent density functional theory study," J. Phys. Chem. C **120**, 28762–28773 (2016).
[54] W. Domcke, D. Yarkony, and H. Köppel, *Conical Intersections: Theory, Computation and Experiment, Advanced Series in Physical Chemistry* (World Scientific Publishing Company, 2011).
[55] M. Tommasini, V. Chernyak, and S. Mukamel, "Electronic density-matrix algorithm for nonadiabatic couplings in molecular dynamics simulations," Int. J. Quantum Chem. **85**, 225–238 (2001).
[56] S. Kilina, E. Badaeva, A. Piryatinski, S. Tretiak, A. Saxena, and A. R. Bishop, "Bright and dark excitons in semiconductor carbon nanotubes: Insights from electronic structure calculations," Phys. Chem. Chem. Phys. **11**, 4113–4123 (2009).
[57] R. J. Magyar and S. Tretiak, "Dependence of spurious charge-transfer excited states on orbital exchange in TDDFT: Large molecules and clusters," J. Chem. Theory Comput. **3**, 976–987 (2007).
[58] N. Oldani, S. Tretiak, G. Bazan, and S. Fernandez-Alberti, "Modeling of internal conversion in photoexcited conjugated molecular donors used in organic photovoltaics," Energy Environ. Sci. **7**, 1175–1184 (2014).
[59] M. Hao, X. Li, K. Shi, D. Xie, X. Zeng, J. Fang, G. Yu, and C. Yang, "Highly efficient photovoltaics and field-effect transistors based on copolymers of monofluorinated benzothiadiazole and quaterthiophene: Synthesis and effect of the molecular weight on device performance," Polym. Chem. **6**, 6050–6057 (2015).
[60] C. Devadoss, P. Bharathi, and J. S. Moore, "Energy transfer in dendritic macromolecules: Molecular size effects and the role of an energy gradient," J. Am. Chem. Soc. **118**, 9635–9644 (1996).
[61] S. F. Swallen, R. Kopelman, J. S. Moore, and C. Devadoss, "Dendrimer photoantenna supermolecules: Energetic funnels, exciton hopping and correlated excimer formation," J. Mol. Struct. **485-486**, 585–597 (1999).
[62] S. Athanasopoulos, L. Alfonso Hernandez, D. Beljonne, S. Fernandez-Alberti, and S. Tretiak, "Ultrafast non-Förster intramolecular donor–acceptor excitation energy transfer," J. Phys. Chem. Lett. **8**, 1688–1694 (2017).
[63] S. Fernandez-Alberti, A. E. Roitberg, V. D. Kleiman, T. Nelson, and S. Tretiak, "Shishiodoshi unidirectional energy transfer mechanism in phenylene ethynylene dendrimers," J. Chem. Phys. **137**, 22A526 (2012).
[64] S. Fernandez-Alberti, V. D. Kleiman, S. Tretiak, and A. E. Roitberg, "Unidirectional energy transfer in conjugated molecules: The crucial role of high-frequency C≡C bonds," J. Phys. Chem. Lett. **1**, 2699–2707 (2010).
[65] D. A. Skoog, F. J. Holler, and S. R. Crouch, *Principles of Instrumental Analysis*, 6th ed. (Thomson Brooks/Cole, Belmont, CA, 2007).
[66] D. F. Eaton, "Reference materials for fluorescence measurement," Pure Appl. Chem. **60**, 1107–1114 (1988).
[67] K. G. Casey and E. L. Quitevis, "Effect of solvent polarity on nonradiative processes in xanthene dyes: Rhodamine B in normal alcohols," J. Phys. Chem. **92**, 6590–6594 (1988).
[68] J. R. Lakowicz, *Principles of Fluorescence Spectroscopy*, 3rd ed., corrected at 4th printing ed. (Springer, New York, 2010).
[69] W. Becker, *Advanced Time-Correlated Single Photon Counting Techniques*, edited by A. W. Castleman, J. Toennies, and W. Zinth Springer Series in Chemical Physics, Vol. 81 (Springer Berlin Heidelberg, Berlin, Heidelberg, 2005).
[70] P. Hanczyc, A. Mikhailovsky, D. R. Boyer, M. R. Sawaya, A. Heeger, and D. Eisenberg, "Ultrafast time-resolved studies on fluorescein for recognition strands architecture in amyloid fibrils," J. Phys. Chem. B **122**, 8–18 (2018).
[71] V. I. Klimov and D. W. McBranch, "Femtosecond high-sensitivity, chirp-free transient absorption spectroscopy using kilohertz lasers," Opt. Lett. **23**, 277 (1998).
[72] T. Nelson, S. Fernandez-Alberti, A. E. Roitberg, and S. Tretiak, "Artifacts due to trivial unavoided crossings in the modeling of photoinduced energy transfer dynamics in extended conjugated molecules," Chem. Phys. Lett. **590**, 208–213 (2013).
[73] T. Nelson, S. Fernandez-Alberti, A. E. Roitberg, and S. Tretiak, "Nonadiabatic excited-state molecular dynamics: Modeling photophysics in organic conjugated materials," Acc. Chem. Res. **47**, 1155–1164 (2014).
[74] S. Tretiak, C. M. Isborn, A. M. N. Niklasson, and M. Challacombe, "Representation independent algorithms for molecular response calculations in time-dependent self-consistent field theories," J. Chem. Phys. **130**, 054111 (2009).
[75] S. Tretiak, V. Chernyak, and S. Mukamel, "Recursive density-matrix-spectral-moment algorithm for molecular nonlinear polarizabilities," J. Chem. Phys. **105**, 8914–8928 (1996).
[76] F. Furche and R. Ahlrichs, "Adiabatic time-dependent density functional methods for excited state properties," J. Chem. Phys. **117**, 7433–7447 (2002).
[77] R. Send and F. Furche, "First-order nonadiabatic couplings from time-dependent hybrid density functional response theory: Consistent formalism, implementation, and performance," J. Chem. Phys. **132**, 044107 (2010).
[78] I. Tavernelli, B. F. E. Curchod, A. Laktionov, and U. Rothlisberger, "Nonadiabatic coupling vectors for excited states within time-dependent density functional theory in the Tamm-Dancoff approximation and beyond," J. Chem. Phys. **133**, 194104 (2010).
[79] S. Mukamel, S. Tretiak, T. Wagersreiter, and V. Chernyak, "Electronic coherence and collective optical excitations of conjugated molecules," Science **277**, 781–787 (1997).
[80] S. Tretiak and S. Mukamel, "Density matrix analysis and simulation of electronic excitations in conjugated and aggregated molecules," Chem. Rev. **102**, 3171–3212 (2002).
[81] D. J. Thouless, *The Quantum Mechanics of Many-Body Systems* (Academic Press, New York, 1972).
[82] S. Tretiak, V. Chernyak, and S. Mukamel, "Two-dimensional real-space analysis of optical excitations in acceptor-substituted carotenoids," J. Am. Chem. Soc. **119**, 11408–11419 (1997).
[83] S. Tretiak, V. Chernyak, and S. Mukamel, "Collective electronic oscillators for nonlinear optical response of conjugated molecules," Chem. Phys. Lett. **259**, 55–61 (1996).
[84] M. G. Paterlini and D. M. Ferguson, "Constant temperature simulations using the Langevin equation with velocity Verlet integration," Chem. Phys. **236**, 243–252 (1998).

[85]P. Attard, "Statistical mechanical theory for non-equilibrium systems. IX. Stochastic molecular dynamics," J. Chem. Phys. **130**, 194113 (2009).
[86]R. Berera, R. van Grondelle, and J. T. M. Kennis, "Ultrafast transient absorption spectroscopy: Principles and application to photosynthetic systems," Photosynth. Res. **101**, 105–118 (2009).
[87]M. Kasha, "Characterization of electronic transitions in complex molecules," Discuss. Faraday Soc. **9**, 14–19 (1950).
[88]T. Nelson, S. Fernandez-Alberti, A. E. Roitberg, and S. Tretiak, "Electronic delocalization, vibrational dynamics, and energy transfer in organic chromophores," J. Phys. Chem. Lett. **8**, 3020–3031 (2018).
[89]M. M. T. El-Tahawy, A. Nenov, O. Weingart, M. Olivucci, and M. Garavelli, "Relationship between excited state lifetime and isomerization quantum yield in animal rhodopsins: Beyond the one-dimensional Landau-Zener model," J. Phys. Chem. Lett. **9**, 3315–3322 (2018).
[90]T. J. Martínez, "Insights for light-driven molecular devices from ab initio multiple spawning excited-state dynamics of organic and biological chromophores," Acc. Chem. Res. **39**, 119–126 (2006).
[91]S. M. Parker, S. Roy, and F. Furche, "Multistate hybrid time-dependent density functional theory with surface hopping accurately captures ultrafast thymine photodeactivation," Phys. Chem. Chem. Phys. **21**, 18999–19010 (2019).
[92]Y. Han, B. Rasulev, and D. S. Kilin, "Photofragmentation of tetranitromethane: Spin-unrestricted time-dependent excited-state molecular dynamics," J. Phys. Chem. Lett. **8**, 3185–3192 (2017).
[93]Z. Lan, E. Fabiano, and W. Thiel, "Photoinduced nonadiabatic dynamics of pyrimidine nucleobases: On-the-fly surface-hopping study with semiempirical methods," J. Phys. Chem. B **113**, 3548–3555 (2009).
[94]S. Ghosh, S. Giannini, K. Lively, and J. Blumberger, "Nonadiabatic dynamics with quantum nuclei: Simulating charge transfer with ring polymer surface hopping," Faraday Discuss. **221**, 501–525 (2020).
[95]A. E. Sifain, J. A. Bjorgaard, T. R. Nelson, B. T. Nebgen, A. J. White, B. J. Gifford, D. W. Gao, O. V. Prezhdo, S. Fernandez-Alberti, A. E. Roitberg, and S. Tretiak, "Photoexcited nonadiabatic dynamics of solvated push-pull π-conjugated oligomers with the NEXMD software," J. Chem. Theory Comput. **14**, 3955–3966 (2018).
[96]J. A. Bjorgaard, V. Kuzmenko, K. A. Velizhanin, and S. Tretiak, "Solvent effects in time-dependent self-consistent field methods. I. Optical response calculations," J. Chem. Phys. **142**, 044103 (2015).
[97]J. A. Bjorgaard, K. A. Velizhanin, and S. Tretiak, "Solvent effects in time-dependent self-consistent field methods. II. Variational formulations and analytical gradients," J. Chem. Phys. **143**, 054305 (2015).
[98]J. A. Bjorgaard, T. Nelson, K. Kalinin, V. Kuzmenko, K. A. Velizhanin, and S. Tretiak, "Simulations of fluorescence solvatochromism in substituted PPV oligomers from excited state molecular dynamics with implicit solvent," Chem. Phys. Lett. **631-632**, 66–69 (2015).
[99]J. A. Bjorgaard, K. A. Velizhanin, and S. Tretiak, "Nonequilibrium solvent effects in Born-Oppenheimer molecular dynamics for ground and excited electronic states," J. Chem. Phys. **144**, 154104 (2016).